Performance Optimization of a Dual Active Bridge Converter Based on Model Predictive Control

Haijun Tian, Mingsuo Yang, Yuepeng Zhang and Zheng Zhou

***Abstract*—A multi-objective optimal control approach is proposed, based on model predictive control (MPC) and extended-phase-shift (EPS) control, to address the transfer efficiency and dynamic performance of the dual active bridge DC-DC converter. Initially, an in-depth analysis of the power characteristics and soft-switching characteristics in each operating mode of the extended phase-shift control is conducted, a mathematical model is formulated, and the Lagrange multiplier method combined with the KKT (Karush-Kuhn-Tucker) condition is used to solve for the combination of phase-shift ratios that minimizes the reflow power. Subsequently, model predictive control is incorporated, which empowers the DAB converter to optimize its dynamic response while enhancing its transmission efficiency. Ultimately, the optimized control strategy is compared and analyzed with the conventional PI control strategy through experiments, and the simulation results show that the optimized strategy based on model predictive control proposed in this paper effectively improves the dynamic performance of the DAB converter under sudden changes in the input voltage, sudden changes in the desired voltage, and sudden changes in the load, and significantly improves the transfer efficiency of the converter, which confirms the validity and superiority of the scheme proposed in this study.**

***Index Terms*—DAB converter, Model predictive control, Dynamic performance, Reflow power, Soft switch**

I. Introduction

With the rise of distributed new energy represented by photovoltaic and wind power, modern microgrids face increasing challenges. Bidirectional DC-DC converters, as a key component of microgrid structure, need to have good steady-state characteristics and dynamic response. Among them, the dual-active-bridge (DAB) converter has become a research hotspot for bidirectional DC-DC converters due to its advantages of high-power density, electrical isolation, and zero-voltage turn-on (ZVS) [1-2].

The single-phase-shift (SPS) modulation method is a widely employed control technique for DAB converters, largely due to its simplicity, which necessitates only a single control variable. However, if the input and output voltages of the DAB converter are not aligned, there may be a notable rise in reflow power and the inability to attain soft switching, which can lead to elevated converter loss and diminished transmission efficiency [3]. In order to overcome the limitations of the SPS modulation method, literature [4] proposes a new phase-shift modulation method called Extend-Phase-Shift (EPS) modulation. This method enhances the system's control flexibility by augmenting the intra-bridge shift ratio within the H-bridge on one side of the DAB converter, thereby expanding the converter's control range. In the studies conducted by In the studies conducted by Literature [5-6], the objective was to optimise reflow power through the utilisation of EPS modulation. The findings suggest that EPS modulation facilitates enhanced system control flexibility, reduces reflow power, and improves system transmission efficiency. In their analysis of the constraints of converter reflow power under EPS modulation, the authors of Literature [7] employed the Karush-Kuhn-Tucker (KKT) method. Subsequently, the optimal phase-shift ratio is employed to attain the minimum reflow power control. The literature [8] proposes an optimal control strategy based on EPS, which is demonstrated to be more effective than the traditional control scheme. Nevertheless, the phase-shift amount specified in this strategy gives rise to a coupling phenomenon, thereby offering scope for further optimisation of the system's dynamic performance. The literature [9] proposes a model prediction scheme under EPS control, establishes the system reflow power expression, and solves the optimal phase shift angle of the converter reflow power through the gradient descent algorithm. This has the potential to significantly reduce the reflow power of the system and thereby enhance its dynamic performance. Nevertheless, the modelling of the system is a challenging task due to the considerable number of parameters involved. Triple-phase-shift (TPS) modulation represents a control strategy that offers a high degree of freedom in phase-shift control. This is due to the presence of intra-bridge shifts in both the primary and secondary sides of the converter, as well as inter-bridge shifts between the primary and secondary sides. In their study, the authors put forth a model prediction-based control method that employs triple phase shift modulation as a means of enhancing the transmission efficiency of the DAB converter. Nevertheless, an increase in the number of control degrees of freedom also results in a greater complexity of system analysis and control, as well as a limitation of the soft-switching range. It is therefore essential to identify a control strategy that simplifies the control method, broadens the soft-switching range, and enhances transmission efficiency and dynamic performance.

In comparison to TPS modulation, EPS modulation exhibits a reduced level of control complexity, with a smaller number of parameters. This feature enables the implementation of an appropriate optimisation control scheme, which serves to enhance transmission efficiency. Accordingly, this paper

Manuscript received June 20, 2024; revised January 27, 2025.

Haijun Tian is a professor at the School of Automation Engineering, Northeast Electric Power University, China 132012. (e-mail: 20101305@neepu.edu.cn).

Mingsuo Yang is a graduate student of Northeast Electric Power University, Jilin City, Jilin Province, China, 132012. (e-mail: cilij5846@163.com).

Yuepeng Zhang is a graduate student of Northeast Electric Power University, Jilin City, Jilin Province, China, 132012. (e-mail: zyp2735@163.com).

Zheng Zhou is a graduate student of Northeast Electric Power University, Jilin City, Jilin Province, China, 132012. (e-mail: 2654933227@qq.com).

examines the reflow power characteristics and soft-switching characteristics of DAB in depth, with reference to the operating principle of DAB under EPS modulation. By employing the Lagrange multiplier method in conjunction with the KKT condition, an optimisation function is constructed to determine the minimum reflow power. Furthermore, model predictive control is employed to enhance the dynamic response of the DAB converter in the presence of diverse, abrupt changes. The proposed scheme is finally validated through the MATLAB/Simulink platform and compared with the traditional PI control strategy.

II. DAB CONVERTER TOPOLOGY AND CHARACTERIZATION

A. Topology of the DAB Converter

Figure 1 illustrates the topology of the DAB converter. In this configuration, the left-hand switching tubes (S_1-S_4) constitute the primary switching bridge H_1, while the right-hand switching tubes (Q_1-Q_4) form the secondary switching bridge H_2. The left side is designated as the input end, while the right side is designated as the output end. The direction of power transmission is from the left to the right, and this is referred to as forward transmission. The input and output voltage sources are designated as U_1 and U_2, respectively. The supply voltage is represented as U_{AB} following the action of bridge H_1, while the load voltage is represented as U_{CD} following the action of bridge H_2. C_1 and C_2 serve as supporting capacitors at the input and output terminals. The inductance, represented by the symbol L, is the sum of the additional inductance and the transformer leakage inductance. The T component in the circuit represents a high-frequency isolation transformer with a ratio of n, which defines the voltage regulation ratio K as $U_1/(nU_2)$. The switching frequency of the switching tube is designated as f, thereby defining the half-switching cycle T_{hs} as 1/(2f). This configuration is symmetric from left to right, and a bidirectional flow of energy can be achieved by controlling the shift ratio between the full bridges H_1 and H_2.

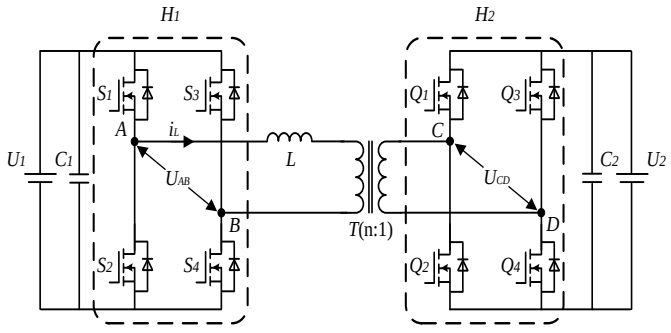

Fig. 1. DAB converter topology diagram.

Fig. 2 illustrates the pulse waveforms as well as the voltage and current waveforms of each switching tube of the DAB converter under EPS modulation. The shift ratio of the primary H_1 bridge under EPS modulation is denoted as D_1, and the external shift ratio between the primary and secondary bridges is denoted as D_2. In light of the fact that the principal analysis of the DAB converter in this study is based on the implementation of EPS modulation, the operating state of the DAB converter can be categorised into two modes on the basis of the relationship between the magnitudes of the shift ratios D1 and D2 in a single switching cycle. These are mode A ($0 \leqslant D_1 \leqslant D_2 \leqslant 1$) and mode B ($0 \leqslant D_2 < D_1 \leqslant 1$).

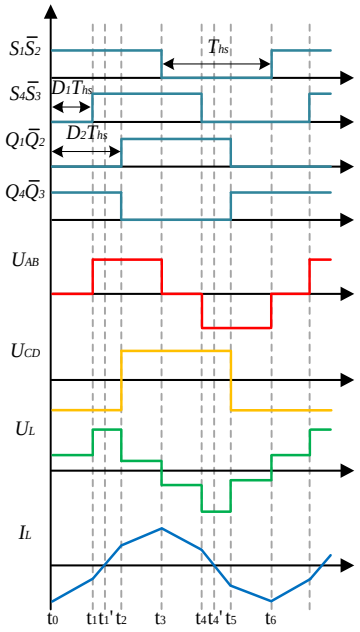

(a) $0 \leqslant D_1 \leqslant D_2 \leqslant 1$

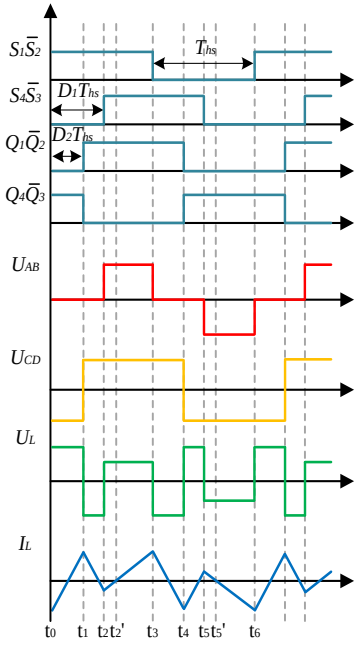

(b) $0 \leqslant D_2 < D_1 \leqslant 1$

Fig. 2. DAB converter working waveform.

A comparison of the two modes of operation waveforms reveals that the different combinations of D1 and D2 caused by the inductor voltage at the two ends of a cycle exhibit a distinct law of change, which in turn gives rise to a divergent trend in the inductor current. The following section presents a mathematical model of the power and soft-switching characteristics of the DAB converter, developed through a comprehensive analysis of its operating principle.

B. Power Characterization of DAB Converter

1) Model A

As shown in Fig. 2(a), when the DAB converter is in steady state under EPS modulation, according to the positive and negative symmetrical characteristics of the inductor current I_L, i.e., $I_L(t_0) = -I_L(t_3)$, and the corresponding shift ratios for each moment in half switching cycle; $t_0 = 0$, $t_1 = D_1 T_{hs}$, $t_2 = D_2 T_{hs}$, and $t_3 = T_{hs}$, the expressions of the inductor currents IL at each moment can be obtained:

$$I_L(t) = \begin{cases} I_L(t_0) = \frac{nU_2}{4Lf}[K(D_1 - 1) - 2D_2 + 1] \\ I_L(t_1) = \frac{nU_2}{4Lf}[K(D_1 - 1) + 2D_1 - 2D_2 + 1] \\ I_L(t_2) = \frac{nU_2}{4Lf}[K(2D_2 - D_1 - 1) + 1] \\ I_L(t_3) = \frac{nU_2}{4Lf}[-K(D_1 - 1) + 2D_2 - 1] \end{cases} \tag{1}$$

This yields an expression for the transmitted power of mode A:

$$\begin{aligned} P_{EPSA} &= \frac{1}{T_{hs}} \int_0^{T_{hs}} U_1 i_L(t) dt \\ &= \frac{nU_1 U_2}{4Lf}(-D_1^2 - 2D_2^2 + 2D_1 D_2 - D_1 + 2D_2) \end{aligned} \tag{2}$$

Defining the maximum transmission power of the DAB converter in the SPS modulation mode, $P_{SPS} = \frac{nU_1 U_2}{8Lf}$ as the reference value, the transmission power scalar value of mode A can be obtained as:

$$P_{EPSA*} = \frac{P_{EPSA}}{P_{SPS}} = 2(-D_1^2 - 2D_2^2 + 2D_1 D_2 - D_1 + 2D_2) \tag{3}$$

Since the reflow power phenomenon occurs during the time period when the primary voltage U_{AB} is in the opposite phase to the inductor current I_L, i.e., the (t_1~t_1') phase of mode A, the mode A reflow power expression can be obtained:

$$\begin{aligned} Q_{EPSA} &= \frac{1}{T_{hs}} \int_{t_1}^{t_1'} U_1 i_L(t) dt \\ &= \frac{nU_1 U_2 [K(D_1 - 1) + 2D_1 - 2D_2 + 1]^2}{16Lf(K + 1)} \end{aligned} \tag{4}$$

The reflow power standard value is:

$$Q_{EPSA*} = \frac{Q_{EPSA}}{P_{SPS}} = \frac{[K(D_1 - 1) + 2D_1 - 2D_2 + 1]^2}{2(K + 1)} \tag{5}$$

2) Model B

Mode B operating waveform is shown in Fig. 2(b), from $t_0 = 0$, $t_1 = D_2 T_{hs}$, $t_2 = D_1 T_{hs}$, and $t_3 = T_{hs}$, the same can be obtained at each moment of the inductor current IL expression is:

$$I_L(t) = \begin{cases} I_L(t_0) = \frac{nU_2}{4Lf}[K(D_1 - 1) - 2D_2 + 1] \\ I_L(t_1) = \frac{nU_2}{4Lf}[K(D_1 - 1) + 1] \\ I_L(t_2) = \frac{nU_2}{4Lf}[K(D_1 - 1) - 2D_1 + 2D_2 + 1] \\ I_L(t_3) = \frac{nU_2}{4Lf}[-K(D_1 - 1) + 2D_2 - 1] \end{cases} \tag{6}$$

Similarly, the transmission power expression for mode B can be obtained:

$$\begin{aligned} P_{EPSB} &= \frac{1}{T_{hs}} \int_0^{T_{hs}} U_1 i_L(t) dt \\ &= \frac{nU_1 U_2}{4Lf}(D_1^2 - D_1 - 2D_1 D_2 + 2D_2) \end{aligned} \tag{7}$$

Then the transmission power of mode B has the following standardized value.

$$P_{EPSB*} = \frac{P_{EPSB}}{P_{SPS}} = 2(D_1^2 - D_1 - 2D_1 D_2 + 2D_2) \tag{8}$$

The reflow power of mode B occurs in the (t2~t2') phase. The expression for the reflow power of mode B can be obtained:

$$\begin{aligned} Q_{EPSB} &= \frac{1}{T_{hs}} \int_{t_2}^{t_2'} U_1 i_L(t) dt \\ &= \frac{nU_1 U_2 [K(D_1 - 1) + 2D_1 - 2D_2 + 1]^2}{16Lf(K - 1)} \end{aligned} \tag{9}$$

Then the mode B reflow power is the standardized value:

$$Q_{EPSB*} = \frac{Q_{EPSB}}{P_{SPS}} = \frac{[K(D_1 - 1) + 2D_1 - 2D_2 + 1]^2}{2(K - 1)} \tag{10}$$

III. Soft-switching characterization of DAB converter

The DAB converter may exhibit a loss of zero-voltage turn-on (ZVS) functionality as a result of the presence of an increased number of switching devices, particularly under specific operational scenarios such as voltage mismatch or light loads and other operating conditions. This can result in a sudden and forceful activation of the switching tubes, leading to an increase in switching losses and a reduction in the converter's transfer efficiency. To enhance the efficiency system transmission and mitigate the loss incurred by the DAB converter, it is imperative to guarantee that all switching tubes are capable of attaining soft switching. The inductor current of the DAB converter exhibits symmetrical characteristics in both positive and negative half-waves. Consequently, when the positive half-week reaches the ZVS point, the negative half-week also attains the ZVS point. It is therefore sufficient to analyse the positive half-week ZVS characteristics.

Referring to Figure 2(a), the ZVS condition for mode A can be observed as follows:

$$\begin{cases} I_L(t_1) \le 0 \\ I_L(t_2) \ge 0 \end{cases} \tag{11}$$

Combining Equation (1) solves the condition in which Mode A achieves the ZVS under EPS Modulation:

$$\begin{cases} D_2 \ge \frac{D_1(K + 2) - K + 1}{2} \\ D_2 \ge \frac{K(D_1 + 1) - 1}{2K} \end{cases} \tag{12}$$

Based on the information provided in Figure 2(b), it can be concluded that the ZVS condition for mode B is:

$$\begin{cases} I_L(t_0) \le 0 \\ I_L(t_1) \ge 0 \\ I_L(t_2) \le 0 \end{cases} \tag{13}$$

Combining equation (6) allows for the determination of the condition where mode B achieves the ZVS under EPS modulation:

$$\begin{cases} D_1 \geq \dfrac{K-1}{K} \\ D_2 \geq \dfrac{K(D_1-1)+1}{2} \\ D_2 \leq \dfrac{D_1(2-K)+K-1}{2} \end{cases} \tag{14}$$

IV. Reflow power optimization control strategy

A. Reflow Power Optimization Scheme

In order for the DAB converter to achieve enhanced efficiency in transmission, it is essential to identify the optimal combination of shift ratio, with the objective of minimizing reflow power while ensuring that the transmission power is satisfied. As previously indicated, the reflow power is influenced by a number of factors, including the transmission power, the ZVS range, and other variables. Consequently, the objective of optimisation is to identify a minimal value of the reflow power, taking into account the aforementioned factors and the transmission power. In comparison with the conventional approach of derivative calculation, the Lagrange multiplier method is more straightforward and comprehensive, thereby significantly reducing the complexity of the calculation process. Accordingly, the Lagrange multiplier method is employed to establish the mathematical relationship between the constraints and the objective function in conjunction with the KKT condition. The constraints and the objective function are combined with the help of the Lagrange multiplier λ and the relaxation variable μ, with the objective of identifying a locally optimal solution of the objective function, which is expressed in general form as follows:

$$\begin{aligned} \min \quad & f(X) \\ s.t. \quad & g_u(X)=0 \quad u=1,2,\cdots,m \\ & h_v(X)=0 \quad v=1,2,\cdots,n \end{aligned} \tag{15}$$

In this context, the objective function is represented by $f(X)$, the equality constraint by $g(X)$, and the inequality constraint by $h(X)$. This method allows the optimisation problem to be converted into a Lagrangian function polynomial solution, with the corresponding functional expression being:

$$L(X,\{\omega_u\},\{\varphi_v\}) = f(X) + \sum_{u=1}^{m} \omega_u g_u(X) + \sum_{v=1}^{n} \varphi_v h_v(X) \tag{16}$$

In this context, ω_u represents the constraint coefficient corresponding to $g_u(X)$, while φ_v denotes the constraint coefficient corresponding to $h_v(X)$. In order to optimise the reflow power, the transmission power is taken as an equal constraint, while the ZVS condition is used as an unequal constraint. The Lagrange polynomials for mode A under EPS modulation are thus established as follows:

$$\begin{aligned} L_A = & \frac{[K(D_1-1)+2D_1-2D_2+1]^2}{2(K+1)} \\ & +[2K(2D_1D_2-D_1^2-2D_2^2-D_1+2D_2)-P] \\ & +\varphi_1[D_1(K+2)-K-2D_2+1] \\ & +\varphi_2[K(D_1+1)-2KD_2-1] \\ & +\varphi_3(-D_1)+\varphi_4(-D_2)+\varphi_5(D_1-1) \\ & +\varphi_6(D_2-1)+\varphi_7(D_1-D_2) \end{aligned} \tag{17}$$

Where P is the given transmission power, the local optimal solution for mode A can be solved as:

$$\begin{cases} D_{11} = \dfrac{(K+1)\sqrt{(1-P)(K^2+2K+2)}}{K^2+2K+2} \\ D_{21} = \dfrac{1}{2} + \dfrac{K\sqrt{(1-P)(K^2+2K+2)}}{2(K^2+2K+2)} \end{cases} \tag{18}$$

According to the constraints of mode A: $0 \leqslant D_1 \leqslant D_2 \leqslant 1$, the range of transmitted power P at this time can be found:

$$\frac{2(K+1)}{(K+2)^2} \leq P \leq 1 \tag{19}$$

Similarly, the Lagrange polynomial for mode B under EPS modulation can be established as:

$$\begin{aligned} L_B = & \frac{[K(D_1-1)+2D_1-2D_2+1]^2}{2(K-1)} \\ & +\omega[2K(D_1^2-D_1-2D_1D_2+2D_2)-P] \\ & +\varphi_1[K(D_1-1)-2D_2+1]+\varphi_2[K-KD_1-1] \\ & +\varphi_3[2D_2-D_1(2-K)-K+1] \\ & +\varphi_4(-D_1)+\varphi_5(-D_2)+\varphi_6(D_1-1) \\ & +\varphi_7(D_2-1)+\varphi_8(D_2-D_1) \end{aligned} \tag{20}$$

The locally optimal solution for mode B is solved as:

$$\begin{cases} D_{12} = 1 - \dfrac{\sqrt{2P(K-1)}}{2(K-1)} \\ D_{22} = \dfrac{1}{2} + \dfrac{(K-2)\sqrt{2P(K-1)}}{4(K-1)} \end{cases} \tag{21}$$

Once more, in accordance with the limitations of mode B ($0 \leqslant D_2 < D_1 \leqslant 1$), the range of the transmitted power P at this juncture can be determined to be:

$$0 \leq P < \frac{2(K-1)}{K^2} \tag{22}$$

Equations (19) and (22) show that the transmission power P is discontinuous in the feasible control domain when the reflow power is at its smallest. To find the optimal solution for the reflow power in the full power range, the critical value of the shift ratio between Mode A and Mode B, D_1=D_2, should be taken. At this point, the transmission power $P_A = P_B$. Subsequently, substitute these values into Eq. (18) to solve the problem:

$$D_{13} = D_{23} = \frac{K+1}{K+2} \tag{23}$$

As illustrated in Fig. 3, the optimal shift ratio combination for reflow power optimisation over the full power range can be derived by combining Eq. (18), Eq. (21), and Eq. (23).

B. Output Voltage Control Scheme Based on Model Predictive Control

Model predictive control (MPC) has been demonstrated to yield superior control performance compared to classical control methods. Its applications in industrial settings, including power converters, attest to its efficacy. Model predictive control entails the construction of a cost function for the discrepancy between the predicted output and the reference value on the basis of a system control model. This is followed by the calculation of the requisite control for the subsequent control cycle, which is achieved by minimising the cost function over the course of each control cycle.

In order to achieve a constant voltage output from the DAB converter, it is necessary to create a model of the output

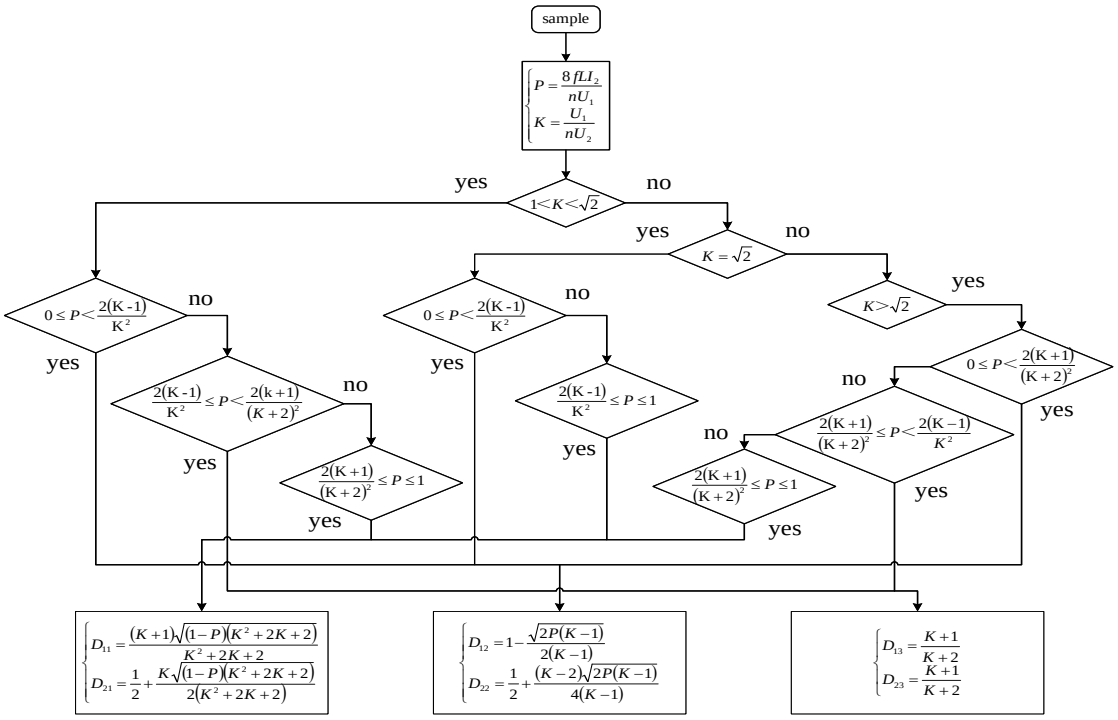

Fig. 3. Flow chart of reflux power optimization control.

voltage with respect to the shift ratio D_1 and D_2. The aforementioned output voltage model will serve as the primary component of the model prediction cost function.

The circuit diagram in Fig. 4 illustrates the analysis of the output circuit. C_2 serves the function of a support capacitor for the output side, while R_O represents the load resistance. The voltage on both sides of R_O represents the output voltage U_2, while nI_{Lavg} denotes the average value of the converter's inductor current normalised to the secondary side.

In accordance with Kirchhoff's current law, the nodal current equation can be formulated as follows:

$$C_2\frac{dU_2}{dt}=I_{C2}=nI_{Lavg}-I_2 \tag{24}$$

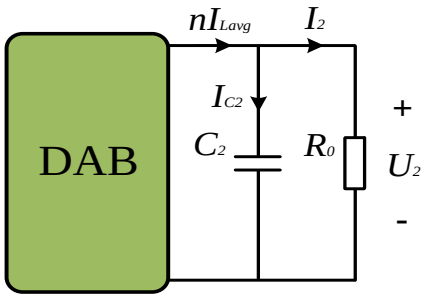

Fig. 4. DAB converter output side circuit diagram.

The switching period of the DAB converter is taken as the control cycle, and it is approximated over the course of one control cycle:

$$C_2\frac{dU_2}{dt}=C_2\frac{U_2(t_{K+1})-U_2(t_K)}{T_S} \tag{25}$$

In the aforementioned equation, $U_2(t_{K+1})$ represents the predicted output voltage following one control cycle, $U_2(t_K)$ denotes the output voltage at the present moment, and T_S signifies the control cycle. The output voltage control equation can be derived by combining the two aforementioned equations:

$$U_2(t_{K+1})=\frac{nI_{Lavg}}{C_2f}-\frac{I_2}{C_2f}+U_2(t_K) \tag{26}$$

Given that I_{Lavg} represents the average current at the output side of the DAB converter and that the inductor current exhibits periodic symmetry, it is sufficient to calculate only half a cycle in order to obtain the equation for the average inductor current in the extended phase-shift modulation mode A:

$$I_{Lavg}=\frac{nU_2(2D_1D_2-D_1^2-2D_2^2-D_1+2D_2)}{4Lf} \tag{27}$$

Similarly, the inductor average current equation can be obtained for the extended phase-shift modulation mode B:

$$I_{Lavg}=\frac{nU_2(D_1^2-2D_1D_2-D_1+2D_2)}{4Lf} \tag{28}$$

The output voltage prediction model of the DAB converter under extended phase shift modulation is obtained by substituting the inductor current averaging equations of extended phase shift modulation mode A and mode B into the output voltage control equation (26), respectively:

$$U_2(t_{K+1})=\begin{cases}U_2(t_K)+\dfrac{n^2U_2(2D_1D_2-D_1^2-2D_2^2-D_1+2D_2)-4LfI_2}{4C_2Lf}\\ U_2(t_K)+\dfrac{n^2U_2(D_1^2-2D_1D_2-D_1+2D_2)-4LfI_2}{4C_2Lf}\end{cases} \tag{29}$$

The constant voltage output of the DAB converter can be realized by taking the target output voltage as U_2^* and solving the following equation:

$$U_2(t_{K+1})-U_2^*=0 \tag{30}$$

The three sets of equations (18), (21), and (23) of the output voltage prediction model and the extended phase-shifted reflow power optimisation model of the DAB converter are solved collectively in order to obtain the hybrid phase-shifted optimisation model, which is then employed in the model predictive control. In conjunction with Fig. 3, the following results emerge:

When $\frac{2(K+1)}{(K+2)^2} < P \le 1$ or $\frac{2(K-1)}{K^2} \le P \le 1$, the extended phase shift optimal shift ratio is:

$$\begin{aligned} D_1 &= \frac{K\sqrt{a_1} + (K^2+2K+2)\sqrt{a_2}}{2(K^2+2K+2)} \\ D_2 &= \frac{(K+1)\sqrt{a_1} + (K^2+2K+2)\sqrt{a_3} + (K^2+2K+2)}{2(K^2+2K+2)} \end{aligned} \tag{31}$$

When $0 \le P < \frac{2(K-1)}{K^2}$ or $0 \le P < \frac{2(K+1)}{(K+2)^2}$, the extended phase-shift optimal shift ratio is:

$$\begin{aligned} D_1 &= \frac{4(K-1) + (K-2)\sqrt{a_4} + 2(K-1)\sqrt{a_5}}{4(K-1)} \\ D_2 &= \frac{\sqrt{a_4} - P + 2(K-1)E}{2\sqrt{a_4}} \end{aligned} \tag{32}$$

When the transmitted power $\frac{2(K-1)}{K^2} \le P < \frac{2(K+1)}{(K+2)^2}$ or $\frac{2(K+1)}{(K+2)^2} \le P < \frac{2(K-1)}{K^2}$, the extended phase-shift optimal shift is compared to:

$$\begin{aligned} D_1 &= \frac{2(K+2) + (K+2)\sqrt{a_6} - K - 2}{2(K+2)} \\ D_2 &= \frac{2(K+2) + (K+2)\sqrt{a_6} - K - 2}{2(K+2)} \end{aligned} \tag{33}$$

In the above equation, $a_1 = (1-P)(K^2+2K+2)$; $a_2 = 1 - 4D_{21}^2 + 4D_{21} - 4E$; $a_3 = 1 - D_{11}^2 - 2E$; $a_4 = 2P(K-1)$; $a_5 = 1 + 4D_{22}^2 - 4D_{22} + 4E$; $a_6 = 1 - 4D_{13}^2 + 4D_{13} - 4E$; $E = \frac{[4KLfI_2 - 4KLC_2f^2(U_2 - U_2^*)]}{nU_1}$.

The aforementioned three sets of equations (Eq. (31), Eq. (32), and Eq. (33)) constitute the model predictive reflow power optimisation model, which represents the core component of the model predictive control system.

V. Simulation Validation

In the preceding section, a model predictive reflow power optimisation model was derived. A simulation model was constructed on the MATLAB/Simulink platform based on the aforementioned model. To ascertain its superiority, a simulation model based on the traditional PI control strategy was also developed for comparison and analysis of the simulation effect of the two schemes. The simulation model of the main circuit of the DAB converter is illustrated in Fig. 5, while the PWM modulation modules based on model predictive control and the one based on conventional PI control are shown in Fig. 6 and Fig. 7, respectively.

The primary simulation parameters of the DAB converter main circuit are presented in Table 1.

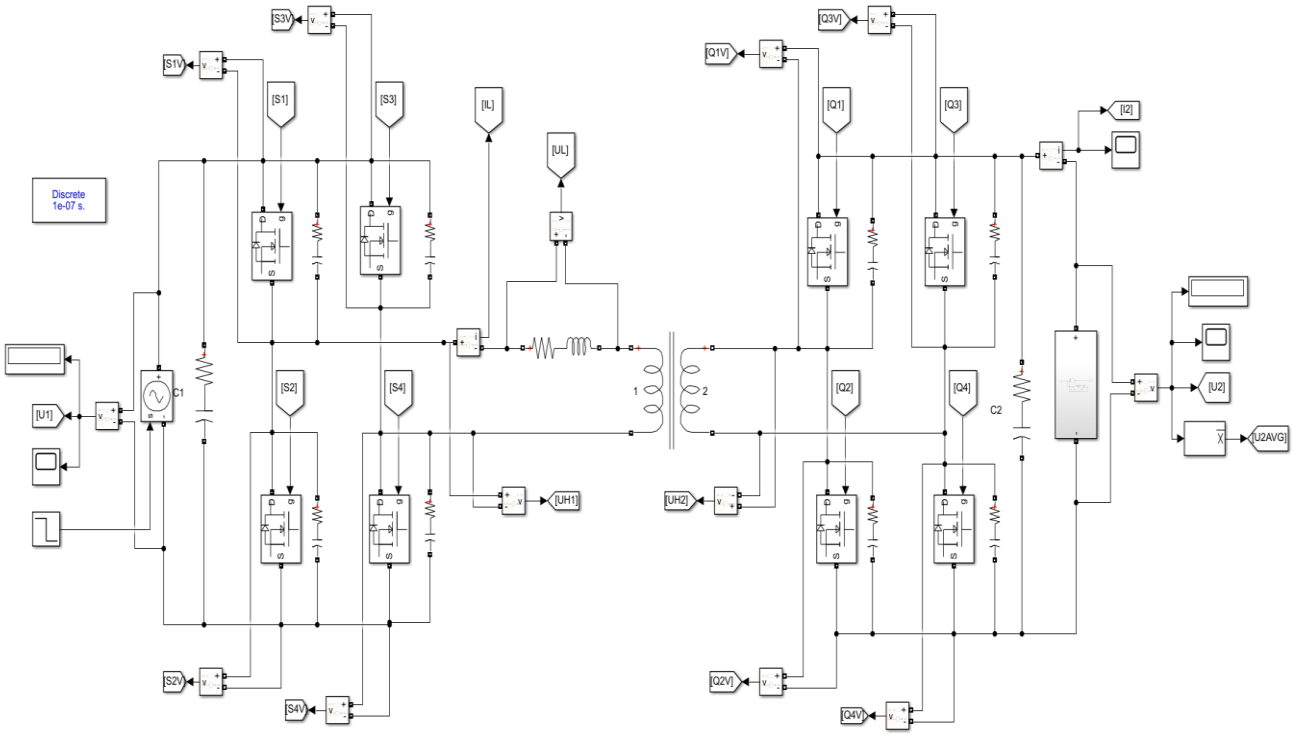

Fig. 5. Simulation Model of DAB Converter Main Circuit.

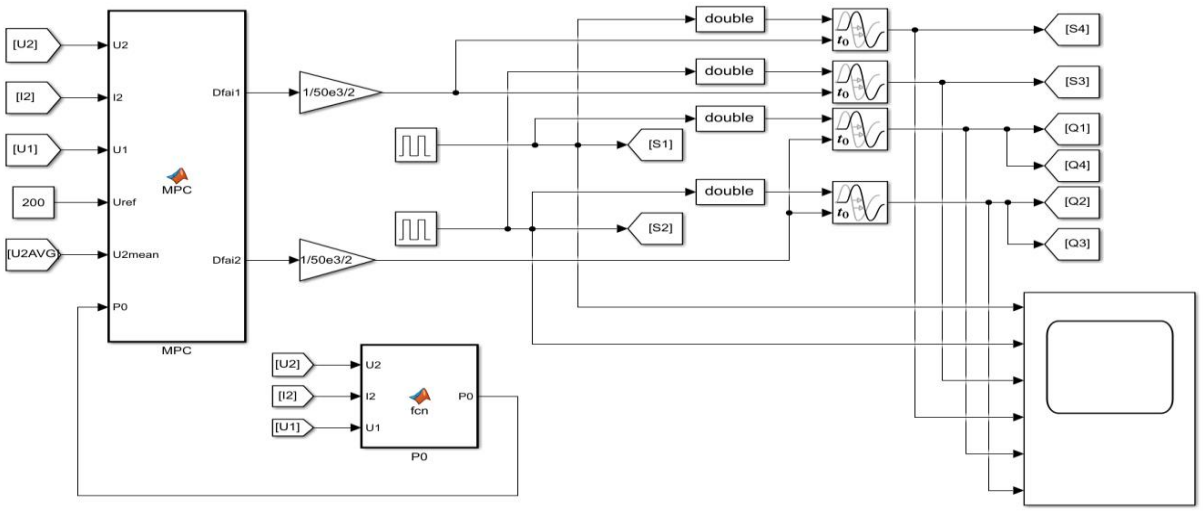

Fig. 6. PWM modulation module based on model predictive control.

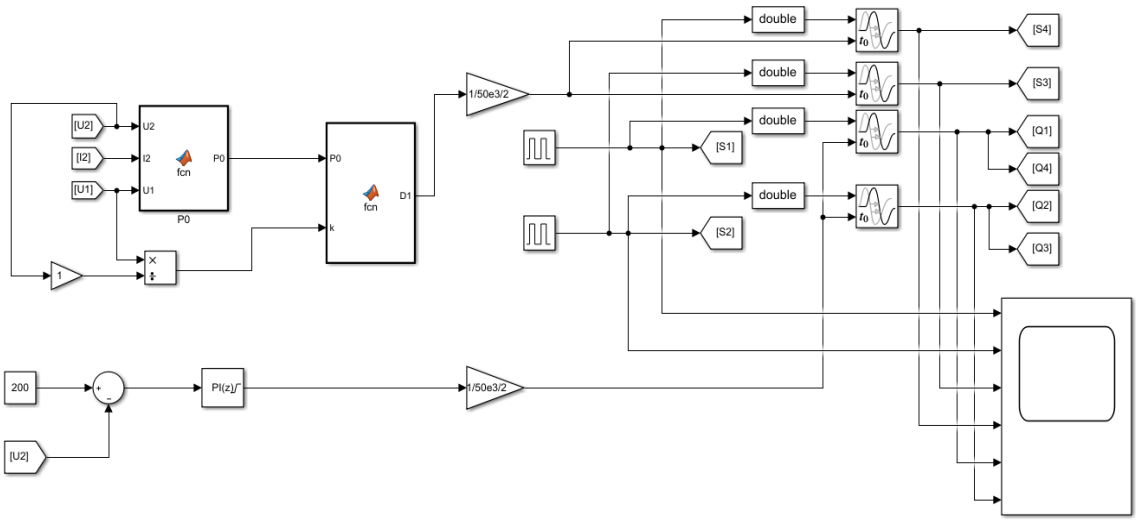

Fig. 7. PWM modulation module based on traditional PI control.

TABLE I
Simulation parameters of DAB converter

Parametric	Numerical Value
Input voltage U_1/V	300
Output voltage U_2/V	200
Inductors L/μH	50
Load resistance R/Ω	180
Capacitors C1、C2/μF	100
Transformer ratio n	1
Switching frequency f/kHz	50

A. Experimental Verification of Dynamic Characteristics

To validate the dynamic response characteristics of the optimized control strategy proposed in this paper, the simulation parameters are set as follows: the input voltage is 300 V, the desired voltage is 200 V, and the load resistance is 180 Ω. The waveforms of the output voltage under the two control schemes are shown in Fig. 8.

From the graph, it can be observed that the traditional PI control strategy exhibits a response time of approximately 60ms and a notable overshoot. In contrast, the model predictive control strategy exhibits a response time of approximately 25ms and no overshoot. Although the output voltage ripple of the model predictive control strategy is marginally larger than that of the traditional PI control strategy, it remains within the 2% limit.

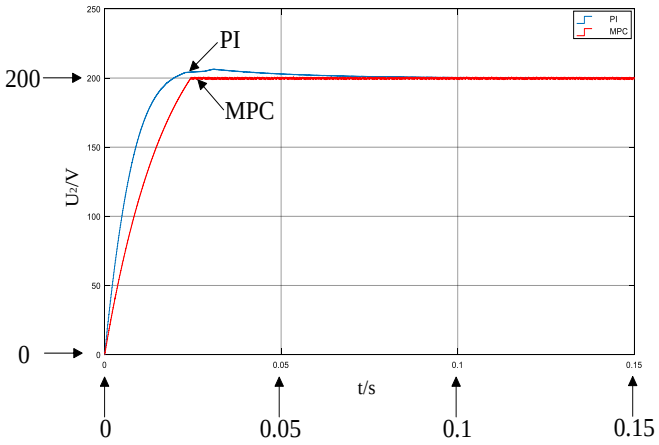

Fig. 8. Dynamic response of output voltage.

When the input voltage is 300 V and the desired voltage is 200 V, the load resistance is switched from 180 Ω to 360 Ω. The output voltage waveforms for the two control strategies are illustrated in Figure 9. From the figure, it can be observed that the traditional PI control strategy exhibits considerable voltage fluctuations in response to sudden load changes. However, following adjustment, it demonstrates a gradual stabilisation in output voltage towards the desired value. In contrast, the model predictive control strategy exhibits minimal voltage fluctuations when tracking the desired value under sudden load changes. The output voltage is maintained at the desired level.

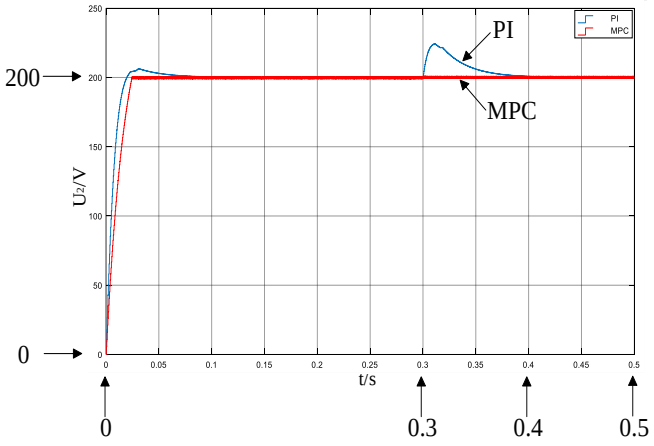

Fig. 9. Sudden change in load resistance.

When the desired voltage is 200 V, the load is 180 Ω, and the input voltage is abruptly changed from 300 V to 240 V, the output voltage waveforms under the two control schemes are illustrated in Fig. 10. The output voltage under the traditional PI control strategy exhibits a voltage fluctuation that persists for approximately 100ms following a sudden change in input voltage before finally stabilising at the desired output voltage. In contrast, the output voltage under the model predictive control strategy demonstrates minimal voltage fluctuation and consistently maintains stability at the specified output voltage. In comparison to the traditional PI control, which necessitates a brief adjustment period, the model predictive control strategy exhibits an almost instantaneous adjustment time and enhanced stability.

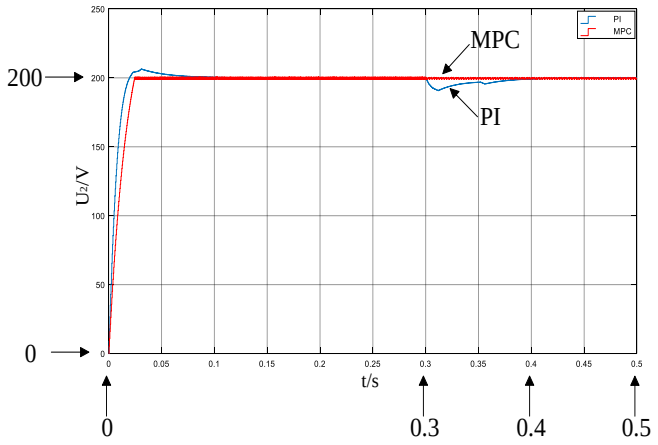

Fig. 10. Input Voltage Surge.

When the input voltage is 300V, the load is 180Ω, and the desired voltage undergoes an abrupt change from 200V to 160V, the output voltage waveforms under the two control schemes are illustrated in Fig. 11. The time required to track the desired value under the traditional PI control strategy when the desired voltage changes abruptly is approximately 55ms. In comparison, the time required to track the desired value under the model predictive control strategy is only 3.5ms. This reduction in time significantly improves the efficiency of the regulation process. In conclusion, both control schemes demonstrate the capacity to respond rapidly to stabilise the output voltage when the desired voltage undergoes an abrupt change. However, the model predictive optimisation control strategy is observed to exhibit superior control efficacy and enhanced dynamic performance.

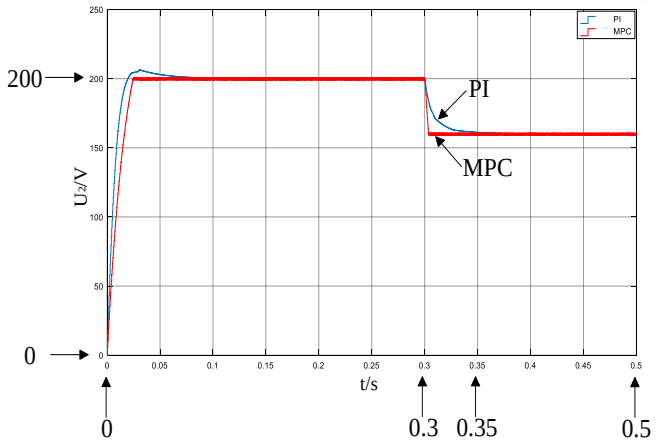

Fig. 11. Desired Voltage Sudden Change.

B. Experimental Verification of Reflow Power Characteristics

Figure 12 illustrates the reflow power simulation waveform of the optimised control strategy proposed in this paper. Figure 13 illustrates the reflow power simulation waveform of the PI control strategy. The phenomenon of reflow power occurs during the period when the primary voltage UAB and the inductor current IL are in opposite phases. Figure 12 demonstrates that the optimal control strategy effectively suppresses reflow power, reducing it to zero. Figure 13 illustrates

that, although the traditional PI control strategy also suppresses reflow power, its suppression effect is more limited and does not reduce reflow power to zero. Consequently, reflow power persists. Thus, a comparison between the traditional PI control reflow power optimisation strategy and the control strategy proposed in this paper reveals that the latter effectively suppresses the reflow power, improves the performance of the DAB converter, and achieves the control requirements.

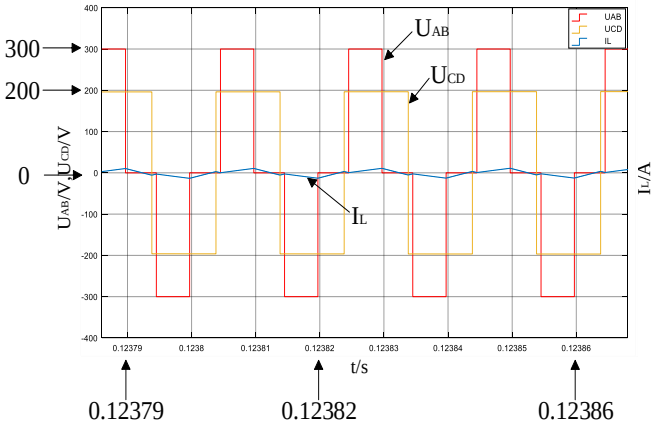

Fig. 12. Simulated waveform of reflow power under optimized control strategy.

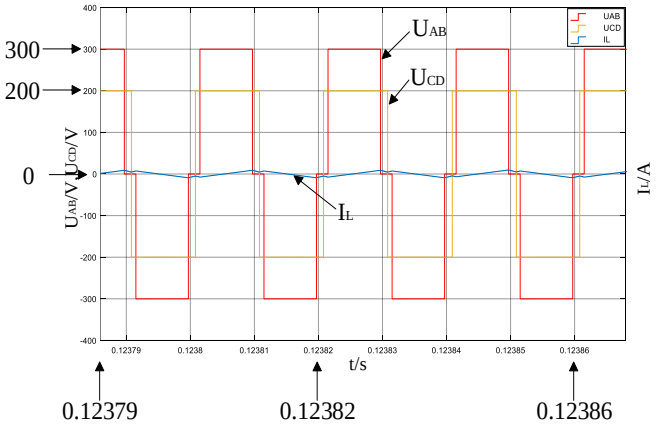

Fig. 13. Simulated waveform of reflow power under PI control strategy.

C. Experimental Verification of Soft-switching Characteristics

Figure 14 shows the synchronized soft switching of all tubes in the DAB converter. The red line shows the amplified tube drive signals, and the blue line shows the voltages on both sides of the tubes. Zero voltage conduction means that the voltage on both sides of the switching tubes drops to zero at the moment of conduction before they are turned on, so it can be seen from Fig. 14 that under the control of the model prediction optimization strategy, the primary side switching tubes (S_1~S_4) and the secondary side switching tubes (Q_1~Q_4) of the DAB converter achieve zero voltage conduction (ZVS) at the same time. This reduces the switching loss of the converter, improves the transmission efficiency of the system, and verifies the effectiveness of the model prediction optimization control strategy.

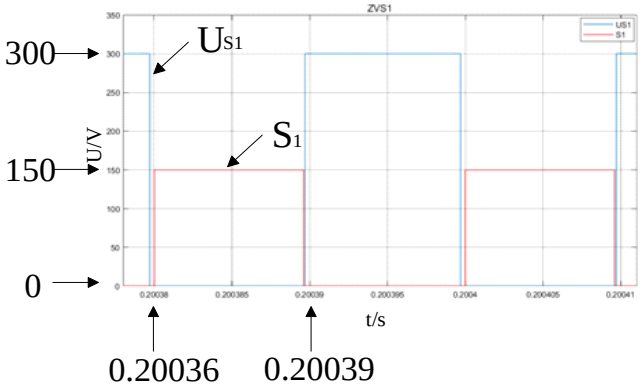

(a) Switching Tube S_1.

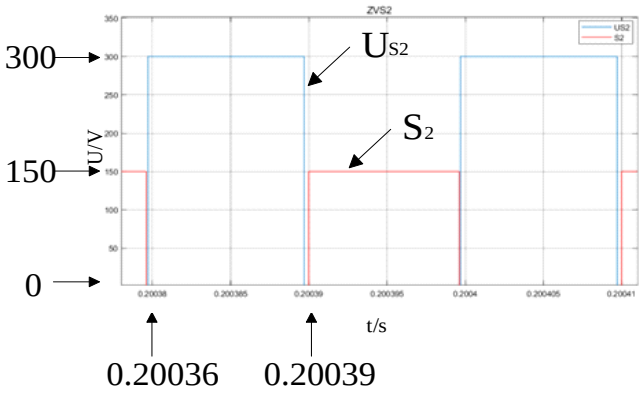

(b) Switching Tube S_2.

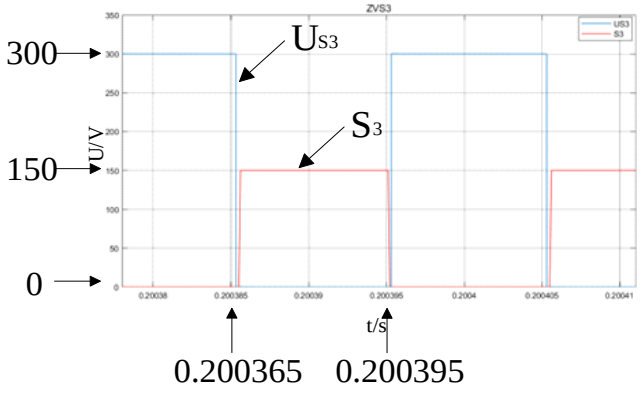

(c) Switching Tube S_3.

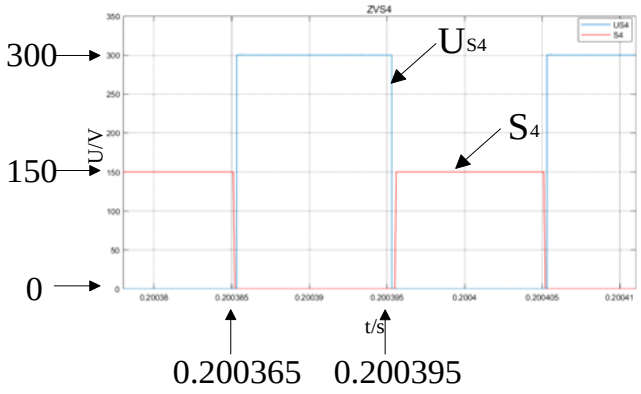

(d) Switching Tube S_4.

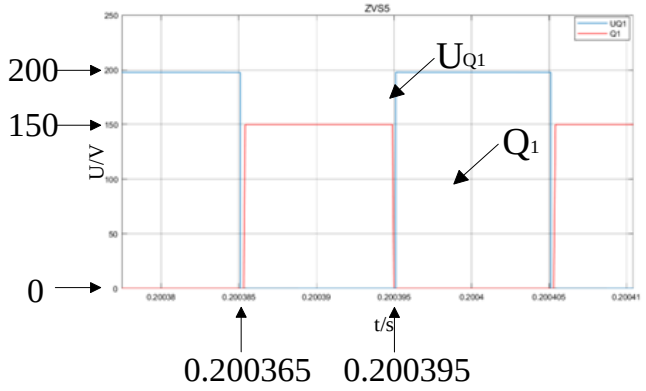

(e) Switching Tube Q_1.

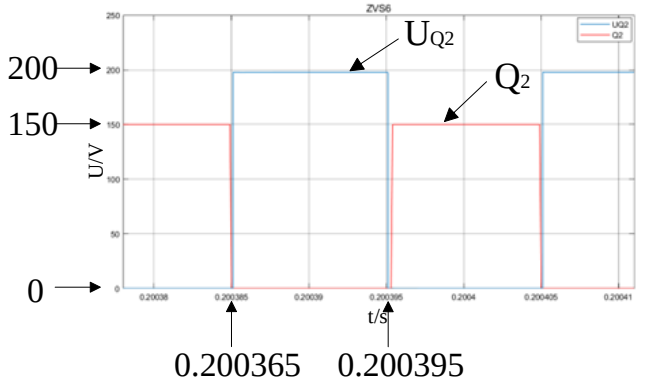

(f) Switching Tube Q_2.

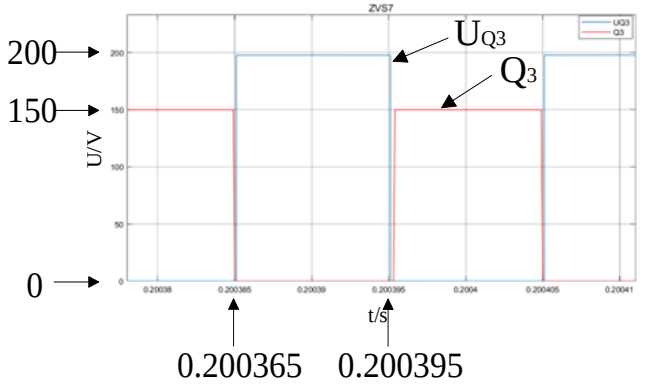

(g) Switching Tube Q_3.

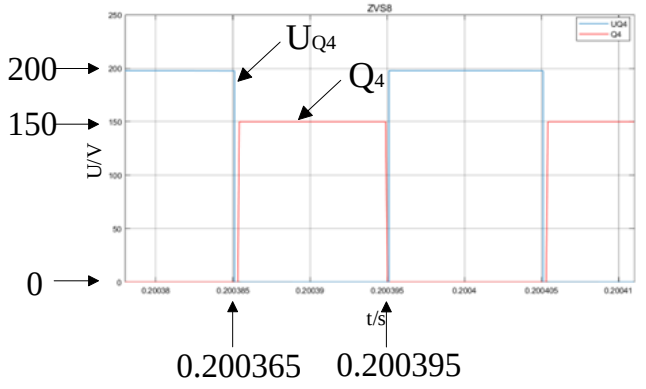

(h) Switching Tube Q_4.

Fig. 14. Soft switching situation of all switch tubes.

D. Experimental Verification of Transmission Efficiency

When the input voltage is 300 V and the load resistance is 180 Ω, Fig. 15 presents a graph of the efficiency of the DAB converter under the two control methods as a function of the output voltage when the reference voltage is gradually increased from 150 V to 240 V. The efficiency of the DAB converter under the two control methods is illustrated in Fig. 25 as a function of the output voltage. As illustrated in the figure, the overall efficiency of the converter declines with an increase in load power. However, it is evident that under the control of the multi-objective optimal control strategy based on model predictive control, the transmission efficiency of the DAB converter is markedly higher than that of the converter under the control of the traditional PI control strategy. This further substantiates the efficacy and soundness of the proposed optimal control strategy.

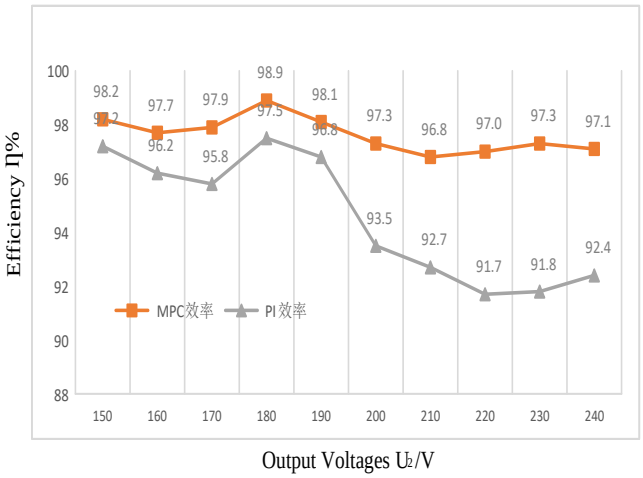

Fig. 15. DAB converter transfer efficiency versus output voltage curves for two control schemes.

VI. Conclusion

This paper presents an analysis of the operational principles of DAB, with a particular focus on its reflow power and soft switching characteristics. To this end, a constraint function is established through the utilisation of the Lagrange multiplier method in conjunction with the KKT condition. Subsequently, Lagrange polynomials are constructed, and optimal solutions are obtained with the reflow power designated as the objective function. Secondly, an output voltage control strategy based on model predictive control is designed to enhance the dynamic performance of the system by incorporating the model predictive control method. Finally, the proposed optimised control strategy is verified in terms of its reliability and superiority, and the simulation effect of the traditional PI control strategy is compared. It can therefore be concluded that, in comparison with the traditional PI control strategy, the proposed model predictive control-based optimal control strategy exhibits superior dynamic performance, a faster response speed and a more stable output in the event of sudden changes. Additionally, the optimised control strategy based on model predictive control is optimised in terms of reflow power and soft switching, which effectively improves the transfer efficiency of the DAB converter. It can therefore be concluded that the optimised control strategy for

the DAB converter proposed in this paper has a certain degree of relevance in practical engineering applications and represents a significant contribution to engineering knowledge.

REFERENCES

[1] Liu H, Lu X, Gao S W, et al. Optimal control of recurrent power of dual active bridge DC-DC converter[J]. Power Supply Technology, 2020, 44(2): 277-281.

[2] Wang P, Chen X, Tong C, et al. Large-and small-signal average-value modeling of dual-active-bridge DC-DC converter with triple-phase-shift control[J]. IEEE Transactions on Power Electronics, 2021, 36(8): 9237-9250.

[3] Sun C, Jiang X, Liu J, et al. A unified design approach of optimal transient single-phase-shift modulation for nonresonant dual-active-bridge converter with complete transient DC-offset elimination[J]. IEEE Transactions on Power Electronics, 2022, 37(11): 13217-13237.

[4] Zhao B, Yu Q, Sun W. Extended-phase-shift control of isolated bidirectional DC-DC converter for power distribution in microgrid[J]. IEEE Transactions on power electronics, 2011, 27(11): 4667-4680.

[5] Tian J, Wang F, Zhuo F, et al. A zero-backflow-power EPS control scheme with multobjective coupled-relationship optimization in DAB-based converter[J]. IEEE Journal of Emerging and Selected Topics in Power Electronics, 2021, 10(4): 4128-4145.

[6] Xu G, Li L, Chen X, et al. Optimized EPS control to achieve full load range ZVS with a seamless transition for dual active bridge converters[J]. IEEE Transactions on Industrial Electronics, 2020, 68(9): 8379-8390.

[7] Guo H, Zhang X, Zhao W G. Optimal Control Strategy of Dual Active Bridge DC-DC Converters With Extended-phase-shift Control[J]. Proceedings of the CSEE, 2019, 39(13): 3889-3898.

[8] Wang P, Li Y P, Fan S W, et al. Research on Optimal Control Strategy of Phase Shift for DAB Converter[J]. Power Electronics, 2021,55(7):117-119.

[9] Zhou B, Yang X, Nong R, et al. Multi-objective optimization control for input-series output-parallel dual-active-bridge DC-DC converter in EER application[C]//2020 IEEE 9th International Power Electronics and Motion Control Conference (IPEMC2020-ECCE Asia). IEEE, 2020: 2408-2413.

[10] Seema Mir Akbar, Ammar Hasan, Alan J. Watson, Pat Wheeler. Model predictive control with triple phase shift modulation for a dual active bridge DC-DC converter[J]. IEEE Access, 2021, 9: 98603-98614.